

## Strain-tunable ferromagnetism and chiral spin textures in two-dimensional Janus chromium dichalcogenides

Qirui Cui,<sup>1,2</sup> Jinghua Liang,<sup>1</sup> Ziji Shao,<sup>1,4</sup> Ping Cui,<sup>1,2</sup> and Hongxin Yang<sup>1,3,\*</sup>

<sup>1</sup>Ningbo Institute of Materials Technology and Engineering, Chinese Academy of Sciences, Ningbo 315201, China

<sup>2</sup>Faculty of Science and Engineering, University of Nottingham Ningbo China, Ningbo, China

<sup>3</sup>Center of Materials Science and Optoelectronics Engineering, University of Chinese Academy of Sciences, Beijing 100049, China

<sup>4</sup>College of Electronics and Information, Hangzhou Dianzi University, Hangzhou, China



(Received 10 May 2020; revised 16 July 2020; accepted 1 September 2020; published 22 September 2020)

Using first-principles calculations and micromagnetic simulations, we systematically investigate the magnetic properties of two-dimensional Janus chromium dichalcogenides ( $\text{CrXTe}$ ,  $X = \text{S, Se}$ ) under strain. We find that the  $\text{CrSTe}$  monolayer has high Curie temperature ( $T_c$ ) of 295 K and an out-of-plane magnetic anisotropy. The  $\text{CrSeTe}$  monolayer has large Dzyaloshinskii-Moriya interaction (DMI) which can host chiral Néel domain wall (DW), and under an external magnetic field, the skyrmion states can be induced. As tensile strain increases, ferromagnetic exchange coupling and perpendicular magnetic anisotropy of Janus  $\text{CrXTe}$  monolayers both increase significantly, and the magnitude of DMI is reduced, which results in the giant ferromagnetism enhancement. Interestingly, for  $\text{CrSeTe}$  monolayer, distinct spin textures from chiral DW to uniform ferromagnetic states are induced under tensile strain. Moreover, the diameter and density of skyrmions in  $\text{CrSeTe}$  can be tuned by the amplitude of external magnetic field and strain. These findings highlight that the Janus  $\text{CrXTe}$  monolayers as good candidates for spintronic nanodevices.

DOI: [10.1103/PhysRevB.102.094425](https://doi.org/10.1103/PhysRevB.102.094425)

### I. INTRODUCTION

Two-dimensional (2D) magnets, which integrates the ideal interface, miniaturization, and long-sought magnetism, provide a fascinating platform for the spintronic research [1–5]. Some exciting phenomena, such as huge tunneling magnetoresistance [6], long-distance magnon transports [7], and magnetization switching driven by spin-orbital torque (SOT) [8], have been realized in the 2D magnets-based device. However, most of these 2D magnets lack high  $T_c$  or large perpendicular magnetic anisotropy (PMA), which are two key parameters in realizing the practical spintronic device with low energy consumption, high thermal stability, and high storage density [8–11]. Therefore, tremendous efforts have been devoted to searching intrinsic 2D magnets with high  $T_c$  and large PMA, or effective method which can enhance these properties [12–14]. Moreover, through breaking the inversion symmetry of 2D magnets, especially constructing the Janus structure [15–17], the sizable Dzyaloshinskii-Moriya interaction (DMI) can be obtained. As an asymmetric exchange interaction induced by spin-orbital coupling (SOC) [18,19], the DMI favors the formation of chiral magnetic structures, such as chiral domain walls and skyrmions, which can be manipulated by small electrical currents and are promising for spintronic applications in the midterm future [20–24]. Furthermore, since the 2D magnets can be integrated into various heterostructures, the chiral spin textures are hopefully tuned by proximity effects.

Magnetic properties are closely related to the structural parameters of materials, and strain can directly influence the structures of materials. Therefore, strain engineering has been shown as an effective method for tuning the magnetic properties [25–27]. In  $\text{FeRh/BaTiO}_3$  heterostructure, the  $\text{FeRh}$  films can be transferred from antiferromagnetic (AFM) to ferromagnetic (FM) order by voltage-induced strain [28] and in  $\text{Fe}_3\text{GeTe}_2$  monolayer, the strain-controlled PMA enhancement has been theoretically predicted [29]. For 2D materials, the lattice strain can be modified through interfacing with various substrates or fabricating stretchable heterostructures [5,30]. These results highlight the possibility of tuning basic magnetic parameters and even inducing distinct spin textures in 2D Janus magnets through strain engineering.

Here, via first-principles calculations and micromagnetic simulations, we systematically investigate the structural and magnetic properties of 2D Janus chromium dichalcogenides  $\text{CrXTe}$  ( $X = \text{S, Se}$ ) under strain.  $1T\text{-CrTe}_2$  bulk is a layered compound and has high  $T_c$  around 310 K [31]. Recently, few-layer  $1T\text{-CrTe}_2$  has been exfoliated from the bulk phase and proved to be able to retain high  $T_c$  [32], which makes Janus  $\text{CrXTe}$  monolayers hopefully fabricated. We find that the  $\text{CrSTe}$  monolayer has high  $T_c$  of 295 K and an out-of-plane magnetic anisotropy. In  $\text{CrSeTe}$  monolayer, the DMI is comparable to that in state-of-the-art FM/heavy-metal (HM) heterostructures, which can favor the formation of chiral domain wall (DW) and skyrmions. As tensile strain increases, the FM exchange coupling and PMA of Janus  $\text{CrXTe}$  monolayers both increase significantly, and the magnitude of DMI is reduced. Therefore, the ferromagnetism of Janus  $\text{CrXTe}$

\*hongxin.yang@nimte.ac.cn

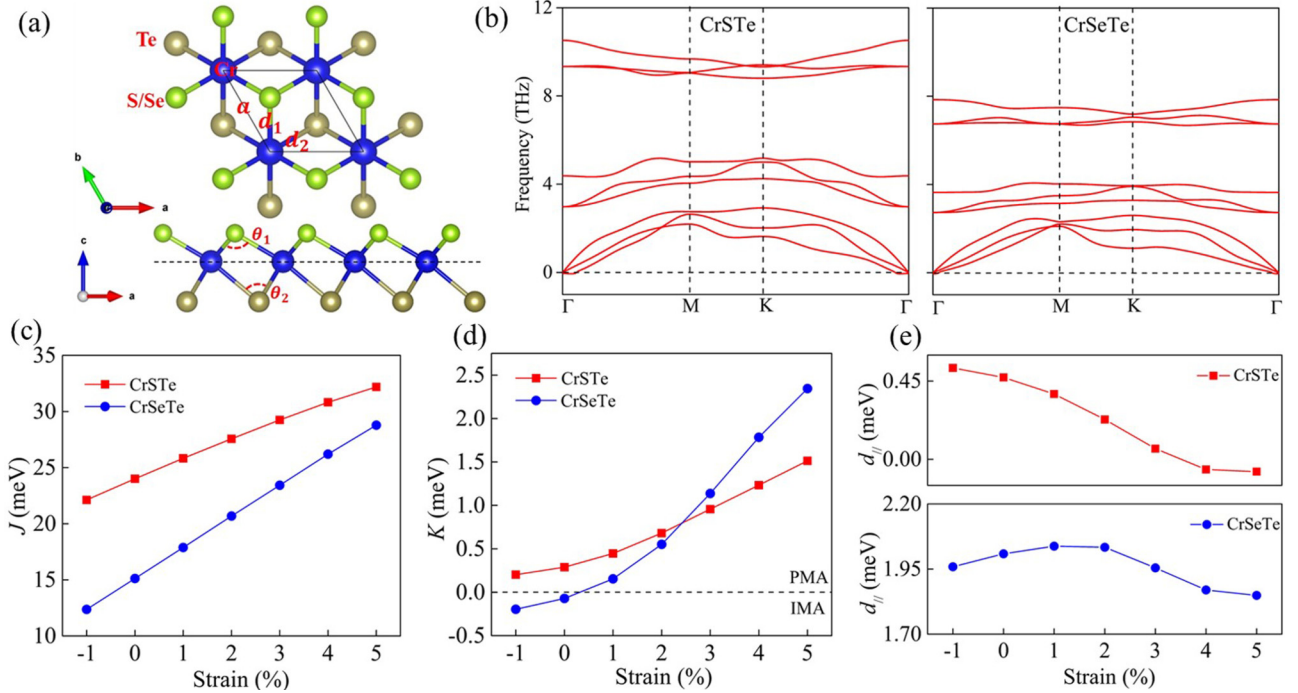


FIG. 1. (a) Top view and side view of crystal structures and (b) Phonon dispersions of Janus CrXTe monolayers. (c) The nearest-neighbor exchange coupling  $J$ , (d) single-ion anisotropy  $K$ , and (e) in-plane DMI component  $d_{\parallel}$  as functions of strain in Janus CrXTe monolayers.

monolayers is obviously enhanced, especially, distinct spin textures are induced in CrSeTe monolayer.

## II. COMPUTATIONAL METHODS

We have performed first-principles calculations within density-functional theory as implemented in the Vienna *Ab initio* Simulation Package (VASP) [33–35]. The exchange-correlation effects are calculated within the generalized gradient approximation (GGA) of Perdew-Burke-Ernzerhof form [36,37]. In order to describe the strongly correlated 3d electrons of Cr, the GGA+ $U$  method is applied ( $U_{\text{eff}} = 2$  eV) [38,39]. The atom positions are fully relaxed until the Hellmann-Feynman force is less than  $10^{-3}$  eV/Å. The cutoff energy is set to 400 eV, and  $\Gamma$ -centered  $24 \times 24 \times 1$   $k$ -point grids are good enough to sample the Brillouin zone. Phonon dispersions are calculated by the PHONOPY code [40]. To investigate the magnetic properties of CrXTe, we adopt the following model Hamiltonian:

$$H = -J \sum_{\langle i,j \rangle} \mathbf{S}_i \cdot \mathbf{S}_j - K \sum_i (S_i^z)^2 - \sum_{\langle i,j \rangle} \mathbf{D}_{ij} \cdot (\mathbf{S}_i \times \mathbf{S}_j) - \mu_{\text{Cr}} B \sum_i S_i^z. \quad (1)$$

In this equation,  $\mathbf{S}_i$  is a unit vector representing the orientation of the spin of the  $i$ th Cr atom, and  $\langle i, j \rangle$  represents the nearest-neighbor Cr atom pairs.  $J$ ,  $K$ , and  $\mathbf{D}_{ij}$  represent the Heisenberg exchange coupling, single-ion anisotropy, and DMI, respectively. The specific method to calculate the  $J$ ,  $K$ , and  $\mathbf{D}_{ij}$  is illustrated in Supplemental Material [41]. The SOC is included in the calculations of the  $K$  and  $\mathbf{D}_{ij}$  except the  $J$ . The SOC effect on  $J$  is also tested. We find that for the pristine

CrS(Se)Te monolayer,  $J = 23.94$  (15.22) meV when SOC is considered, which is very close to  $J = 24.00$  (15.11) meV without SOC. The sign convention is that  $J > 0$  represents FM coupling,  $K > 0$  refers to PMA, and in-plane DMI component  $d_{\parallel} > 0$  favors clockwise (CW) spin configurations. Based on calculated magnetic parameters, the Monte Carlo (MC) simulations with Metropolis algorithm [42] are applied to explore the spin textures and estimate  $T_c$  of CrXTe. The details of MC simulations are given in Supplemental Material [41]. The value of strain is defined as  $(a - a_0)/a_0$ , where  $a$  and  $a_0$  are the lattice constants of strained and unstrained CrXTe monolayers.

## III. RESULTS AND DISCUSSION

The crystal structure of CrXTe monolayers is shown in Fig. 1(a). The Cr atoms in central layer form a triangular lattice with  $C_{6v}$  symmetry, and after sandwiched by two atomic layers of different chalcogen atoms represented by light-green (X) and dark-green (Te) balls, the overall symmetry reduces to  $C_{3v}$ . The optimized structural parameters of CrXTe monolayers and magnetic moments of Cr, X, and Te atoms are listed in Table I. The optimized lattice constant of CrSTe is smaller than CrSeTe, due to the smaller atomic radii of S compared with that of Se. With the same computational method and accuracy, we also obtain the lattice constant of CrTe<sub>2</sub> monolayer, 3.70 Å, which yields good comparison with the experimental value of CrTe<sub>2</sub> bulk, 3.79 Å [31]. One can see that the lattice constant of CrSTe and CrSeTe is smaller than CrTe<sub>2</sub> due to the largest radii of Te among the S, Se, and Te. For a specific CrXTe monolayer, the atomic radii of Te are larger than those of X. Therefore,  $d_1$  and  $\theta_2$  are always smaller than  $d_2$  and  $\theta_1$ , respectively. The difference of top and bottom atom layer

TABLE I. The optimized lattice constants  $a$ , bond length of Cr- $X$   $d_1$ , and Cr-Te  $d_2$ , bonding angle of Cr- $X$ -Cr  $\theta_1$  and Cr-Te-Cr  $\theta_2$ , and magnetic moments of Cr  $\mu_{\text{Cr}}$ , S  $\mu_{\text{S}}$ , Se  $\mu_{\text{Se}}$ , and Te  $\mu_{\text{Te}}$  of Janus Cr $X$ Te monolayer. The unit of  $a$ ,  $d_1$ , and  $d_2$  is Å. The unit of  $\theta_1$  and  $\theta_2$  is deg. The unit of  $\mu_{\text{Cr}}$ ,  $\mu_{\text{S}}$ ,  $\mu_{\text{Se}}$ , and  $\mu_{\text{Te}}$  is  $\mu_{\text{B}}$ . The opposite sign of magnetic moment between S, Se, Te, and Cr atoms reveals that the exchange coupling between them is AFM.

	$a$	$d_1$	$d_2$	$\theta_1$	$\theta_2$	$\mu_{\text{Cr}}$	$\mu_{\text{S}}$	$\mu_{\text{Se}}$	$\mu_{\text{Te}}$
CrSTe	3.47	2.34	2.84	95.66	75.22	3.13	-0.20		-0.15
CrSeTe	3.56	2.48	2.82	91.67	78.26	3.20		-0.25	-0.18

induces inversion symmetry breaking in Cr $X$ Te monolayer, which is essential for DMI. The main contribution to magnetism of Cr $X$ Te comes from the Cr atoms, meanwhile,  $X$  and Te are both effectively spin polarized due to proximity effects. To confirm the structural stability of Cr $X$ Te monolayers, we calculate phonon spectra as shown in Figs. 1(b) and 1(c). One can see that there is no imaginary frequency in the Brillouin zone, which suggests that Cr $X$ Te monolayers are dynamically stable. Furthermore, to investigate electronic states of Cr $X$ Te monolayers, we calculate the orbital and spin-projected band structures as shown in Fig. S3. The band structures show that Cr $X$ Te monolayers are metallic. For spin-up channel, the occupied states are dominated by  $3d$  electrons of Cr. However, for spin-down channel, the occupied states mainly come from  $p$  states of  $X$  and Te. These results are consistent with the opposite spin orientations between Cr and  $X$ , Te as shown in Table I.

Now we focus on the magnetic interaction parameters including  $J$ ,  $K$ , and  $d_{\parallel}$ , and their change under strain. As shown in Fig. 1(c), the nearest-exchange coupling of CrS(Se)Te monolayer is FM and when the tensile strain increases from 0 to 5%, the magnitude of this FM coupling can be effectively enhanced from 24.00 (15.11) to 32.19 (28.78) meV. Figure 1(d) shows  $K$  of Cr $X$ Te as a function of strain. One can see that pristine CrSTe has PMA of 0.29 meV, and CrSeTe has in-plane magnetic anisotropy (IMA) of 0.07 meV. Interestingly, by just 5% tensile strain, the PMA of CrS(Se)Te can be significantly enhanced to 1.51 (2.35) meV, which is much larger than that of CrI<sub>3</sub>, 0.80 meV [38]. We find that Cr $X$ Te monolayers have sizable DMI as shown in Fig. 1(e). Especially, the  $d_{\parallel}$  of pristine CrSeTe monolayer reaches to 2.01 meV, which is comparable to state-of-the-art FM/HM heterostructures, such as Pt/Co ( $\sim 3.0$  meV) [43] and Fe/Ir(111) ( $\sim 1.7$  meV) [44], thin films that have been demonstrated to be able to host chiral spin textures. One also can see that the tensile strain reduces the magnitude of  $d_{\parallel}$  of both CrSTe and CrSeTe monolayers. For the CrTe<sub>2</sub> monolayer,  $J = 2.16$  meV,  $K = -2.14$  meV, and  $d_{\parallel} = 0$  meV. One can see that, compared with the CrTe<sub>2</sub> monolayer, the FM coupling and IMA is obviously increased and decreased, respectively, in Janus structures, which is more beneficial for the formation of long-range magnetic order.

The physical mechanisms of the change of  $J$  and  $K$  under strain are similar for CrSTe and CrSeTe. Therefore, in the following discussion, we choose CrSeTe as an example to show in detail how tensile strain enhances the FM coupling

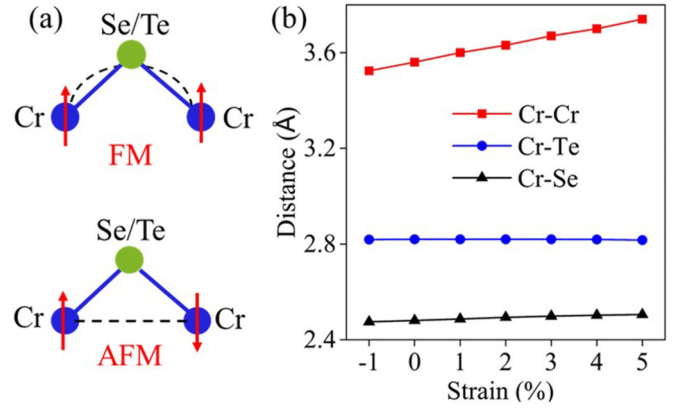


FIG. 2. (a) Schematic diagrams of Cr-Se/Te-Cr superexchange and Cr-Cr direct exchange couplings in Janus CrSeTe monolayer. (b) Bond lengths of Cr-Cr, Cr-Te, and Cr-Se as functions of the strain.

and PMA. Since the bonding angle of Cr-Se/Te-Cr is close to  $90^\circ$ , according to the Goodenough-Kanamori-Anderson rules [45–47], the indirect exchange coupling between two nearest-neighbor Cr cations through intervening Se/Te anion is FM [upper panel of Fig. 2(a)]. On the contrary, the direct exchange coupling between two nearest-neighbor Cr cation is AFM [lower panel of Fig. 2(a)]. The competition between indirect FM and direct AFM couplings decides the final magnetic arrangement of Cr atoms. When tensile strain is applied, the Cr-Te and Cr-Se distances hardly change [blue and black line in Fig. 2(b)], whereas the Cr-Cr distance obviously increases [red line in Fig. 2(b)]. Therefore, compared with indirect FM coupling, the direct AFM coupling decreases more strongly, which results in the effective enhancement of  $J$  [48].

From the atom-resolved magnetic anisotropy energy (MAE) of the CrSeTe monolayer [Fig. 3(a)], one can see that the PMA of Te atom is enhanced significantly by tensile strain, which is responsible for the  $K$  increasing. To further elucidate mechanisms of MAE change of Te atom, we perform a comparative analysis of MAE from orbital hybridization between the CrSeTe monolayer under 0 and 5% tensile strain as shown in Figs. 3(b) and 3(c). For Te in pristine CrSeTe, the hybridization between  $p_y$  and  $p_x$  gives rise to IMA; however, the hybridization between  $p_y$  and  $p_z$  constitutes PMA. The small magnitude of anisotropy of Te in pristine CrSeTe arises from the competition of these two hybridizations. When the strain is applied on the CrSeTe, the PMA contribution comes from the  $p_y$  and  $p_z$  hybridization, significantly increases, and the IMA contribution arising from  $p_y$  and  $p_x$  hybridization hardly changes, which results in the giant PMA enhancement of the CrSeTe monolayer. Furthermore, we investigate the origin of the change of MAE arising from  $5p$  orbital hybridization of the Te atom. According to the second-order perturbation theory [49,50], the MAE can be expressed as

$$\text{MAE} = \xi^2 \sum_{\sigma\sigma'} \sum_{\sigma''\sigma'''} \frac{(2\delta_{\sigma\sigma''} - 1)(|\langle \sigma'' | L_z | \sigma'' \rangle|^2 - |\langle \sigma'' | L_x | \sigma'' \rangle|^2)}{E_u^{\sigma''} - E_o^{\sigma''}}. \quad (2)$$

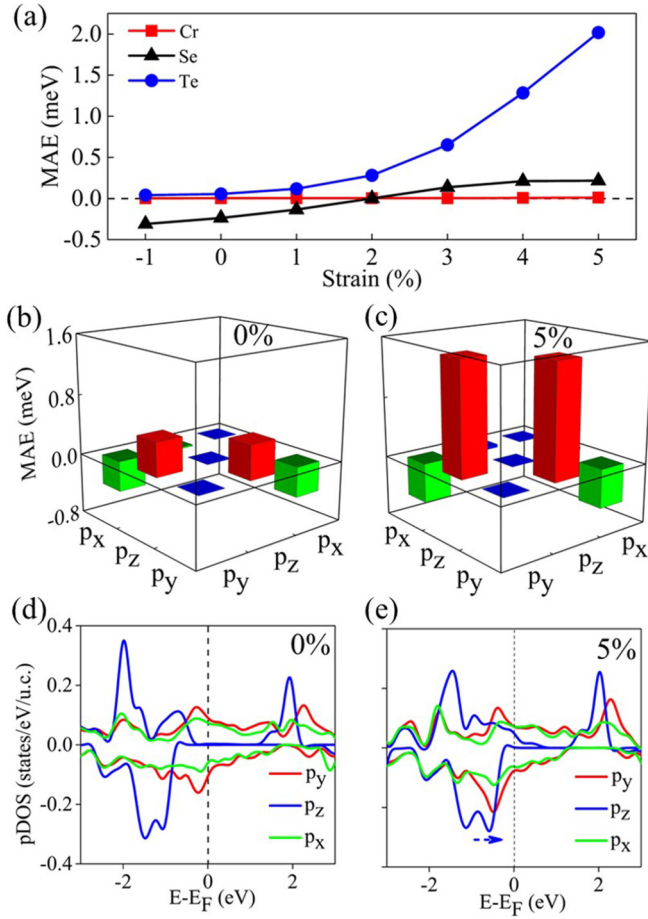


FIG. 3. (a) Atom-resolved MAE of Janus CrSeTe monolayer as functions of the strain. (b), (c) MAE contributions from  $5p$  orbitals hybridization, and (d), (e) the projected density of states of Te in Janus CrSeTe monolayer under 0 and 5% tensile strain.

$\xi$  represents the SOC amplitude.  $E_u^{\sigma'}$  and  $E_o^{\sigma}$  are the energy levels of unoccupied states with spin  $\sigma'$  and occupied states with spin  $\sigma$ , respectively.  $(2\delta_{\sigma\sigma'} - 1)(|o^{\sigma}| |L_z |u^{\sigma'}|^2 - |o^{\sigma'}| |L_x |u^{\sigma}|^2)$  is the difference of spin-orbital angular momentum matrix elements, which is shown in Table SI. In Figs. 3(d) and 3(e), we plot the projected density of states for Te atoms of CrSeTe monolayers under 0 and 5% tensile strain. One can see that the spin-down occupied  $p_z$  states ( $p_z^{\sigma-}$ ) is shifted to the Fermi level  $E_F$  [indicated by the dashed blue arrow in Fig. 3(e)] when tensile strain is enhanced. The matrix elements difference between  $p_z^{\sigma-}$  and spin-up unoccupied  $p_y$  states ( $p_y^{\sigma+}$ ) is 1 as shown in Table SI, which is responsible for the PMA contribution from  $p_y$  and  $p_z$  hybridization. Due to the shift of  $p_z^{\sigma-}$  states, the value of  $E_u^{\sigma'} - E_o^{\sigma}$  obviously decreases. Therefore, the positive MAE from  $p_y$  and  $p_z$  hybridization is enhanced. Compared with  $p_z$  states, the  $p_x$  and  $p_y$  states barely change, which is responsible for the much smaller variation of MAE from  $p_x$  and  $p_y$  hybridization.

For investigating the exceptional DMI in CrXTe monolayer, we calculate SOC energy difference  $\Delta E_{\text{soc}}$  of the opposite chirality as shown in Fig. 4. One can see that the dominant contribution to the DMI stems from the adjacent  $X$  and Te atoms. This behavior is similar to DMI

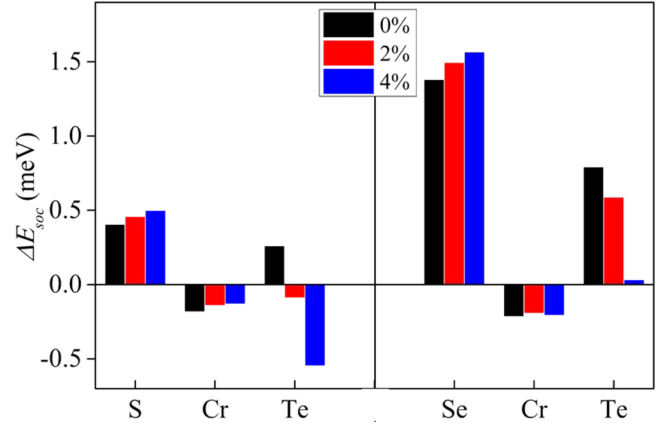


FIG. 4. Atom-resolved localization of the SOC energy difference  $\Delta E_{\text{soc}}$  in Janus CrXTe monolayer. Black, red, and blue bars represent  $\Delta E_{\text{soc}}$  of CrXTe monolayers under 0, 2, and 4% tensile strain, respectively.

in FM/HM heterostructures, where the SOC energy source comes from  $5d$  transition metal in the interfacial layer. This is the so-called Fert-Levy type of DMI [51,52]. In CrXTe monolayer, when polarized electrons transfer between Cr atoms through mediate  $X$ /Te atoms, the spin orientations of these electrons can be tilted due to the spin-orbit scattering [51]. Under tensile strain, the Te contribution to DMI of CW chirality obviously decreases, which is responsible for the reduction of total DMI magnitude.

Once magnetic interaction parameters of spin Hamiltonian are determined by first-principles calculation, we perform MC simulations to explore the spin textures and  $T_c$  of Janus CrXTe monolayers. We notice that the DMI/exchange coupling ratios  $|d_{\parallel}/J|$  of pristine CrSeTe monolayer is about 0.14, which is in the typical range of 0.10–0.20 for the skyrmions formation [53]. Therefore, it is possible to realize chiral spin textures in CrSeTe monolayer. Figure 5(a) shows a phase diagram of spin textures of CrSeTe monolayer in 10 K. For pristine CrSeTe, we obtain the wormlike domains separated by chiral Néel DW, the white part between the domains of up and down magnetization. Due to the in-plane magnetic anisotropy, the width of DW reaches to 2.7 nm. We find that the skyrmion states can be induced in pristine CrSeTe by external magnetic field ( $B_z$ ). One can see that the red domains shrink as the enhancement of  $B_z$  and isolated skyrmions begin to appear. When the  $B_z$  increases to 1.2 T, the worm domains disappear completely and the skyrmions tend to form an approximate hexagonal lattice. If we keep increasing  $B_z$ , the density of skyrmions decreases and a uniform ferromagnetic state appears finally. The diameter of skyrmions decreases from 11.6 to 9.1 nm when  $B_z$  increases from 1.2 to 2.1 T.

As tensile strain increases, the size of domain in CrSeTe becomes much larger compared with pristine state, which is consistent with the smaller  $|d_{\parallel}/J|$ , and the resulting larger DW energy. Meanwhile, the width of DW decreases obviously induced by transition of IMA to large PMA in CrSeTe. Due to the enhancement of ferromagnetic exchange coupling and PMA, the critical external field required for skyrmions formation, density, and diameters of skyrmions all decrease. When tensile strain reaches up to 3%, the  $|d_{\parallel}/J|$  decreases to 0.08,

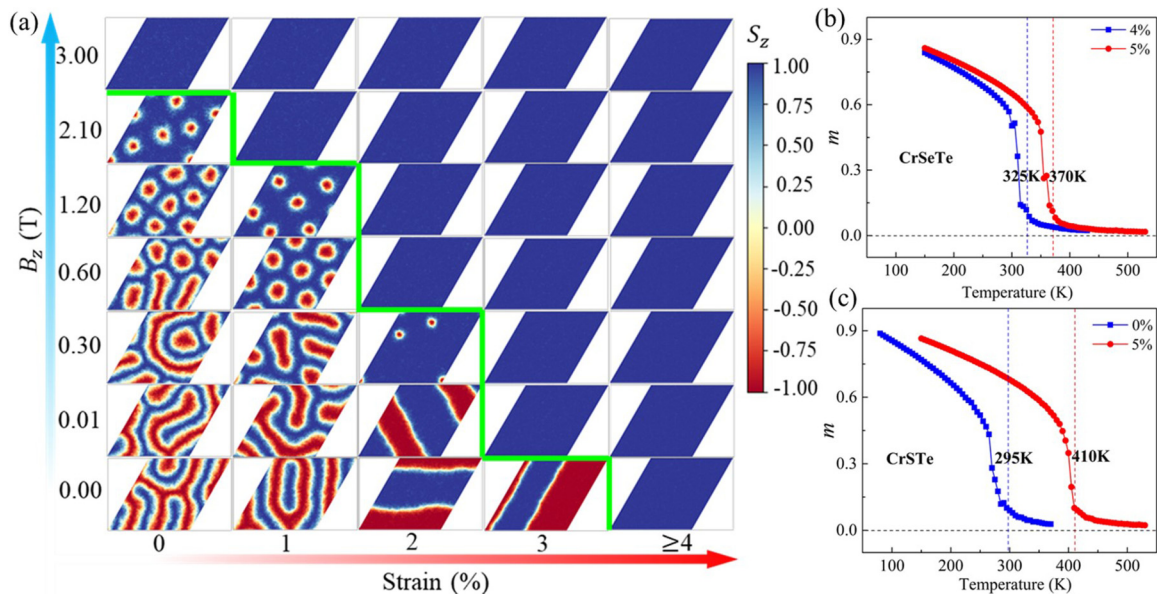


FIG. 5. (a) Distinct spin textures for CrSeTe monolayer under increased tensile strains and external fields in 10 K. The color map indicates the out-of-plane spin component of Cr atoms. The curie temperatures ( $T_c$ ) of (b) CrSeTe and (c) CrSTe monolayers under tensile strains.

which is not in typical range for skyrmions formation. Therefore, the DW directly transforms into uniform ferromagnetic state under a very small  $B_z$ , 0.01 T. If we keep increasing tensile strain above 3%, the uniform ferromagnetic states appear. Moreover, these ferromagnetic states can retain over 325 K as shown in Fig. 5(b). Next, we explore the temperature influence on spin textures as shown in Figs. S4(a) and S4(b). One can see that the images of chiral domain wall, skyrmions, and uniform ferromagnetic states all begin to be less well-defined and become more and more blurred as temperature increases. When  $T$  increases to 150 K, this blurring starts to show the destabilization of chiral spin textures by thermal fluctuations, but the tendency of the evolution of chiral spin textures with external magnetic field or tensile strain is still clear. For CrSTe monolayer, the magnetic ground state is ferromagnetic without chiral spin textures, which is consistent with the very small  $|d_{||}/J|$  of 0.02. Notably, the  $T_c$  of pristine CrSTe reaches to 295 K [blue line in Fig. 5(c)] which is close to room temperature, and it can be further enhanced to 410 K when tensile strain increases to 5% [red line in Fig. 5(c)].

#### IV. CONCLUSIONS

In summary, using first-principles calculations and MC simulations, we systematically investigate magnetic proper-

ties of Janus CrXTe monolayers. We find that the CrSTe monolayer has a high  $T_c$  of 295 K and an out-of-plane magnetic anisotropy. The CrSeTe monolayer has large DMI, which favors the formation of chiral Néel DW. With an external magnetic field, the DW in CrSeTe can be tuned to skyrmion states. As tensile strain increases, the FM exchange coupling and PMA of Janus CrXTe monolayers increase significantly, and the magnitude of DMI is reduced. Therefore,  $T_c$  of CrSTe is enhanced over 100 K under 5% tensile strain, and in CrSeTe, distinct spin textures from chiral Néel domain wall to uniform ferromagnetic states are induced. Moreover, the diameter and density of skyrmions in CrSeTe monolayer can be tuned by external magnetic field and strain. Our results provide good candidates for experimental investigation of 2D Janus magnets, which is helpful for spintronic applications.

#### ACKNOWLEDGMENTS

This work was supported by the Key Research Program of Frontier Sciences, CAS, Grant No. ZDBS-LY-7021, National Natural Science Foundation of China (Grant No. 11874059), Zhejiang Province Natural Science Foundation of China (Grant No. LR19A040002), and Ningbo 3315 project.

- [1] C. Gong, L. Li, Z. Li, H. Ji, A. Stern, Y. Xia, T. Cao, W. Bao, C. Wang, Y. Wang, Z. Q. Qiu, R. J. Cava, S. G. Louie, J. Xia, and X. Zhang, *Nature (London)* **546**, 265 (2017).  
 [2] B. Huang, G. Clark, E. N. Moratalla, D. R. Klein, R. Cheng, K. L. Seyler, Ding Zhong, E. Schmidgall, M. A. McGuire, D. H. Cobden, W. Yao, D. Xiao, P. J. Herrero, and X. Xu, *Nature (London)* **546**, 270 (2017).

- [3] K. S. Burch, D. Mandrus, and J.-G. Park, *Nature (London)* **563**, 47 (2018).  
 [4] M. Slota, A. Keerthi, W. K. Myers, E. Tretyakov, M. Baumgarten, A. Ardavan, H. Sadeghi, C. J. Lambert, A. Narita, K. Müllen, and L. Bogani, *Nature (London)* **557**, 691 (2018).  
 [5] C. Gong and X. Zhang, *Science* **363**, eaav4450 (2019).

- [6] T. Song, X. Cai, M. W. Tu, X. Zhang, B. Huang, N. P. Wilson, K. L. Seyler, L. Zhu, T. Taniguchi, K. Watanabe, M. A. McGuire, D. H. Cobden, D. Xiao, W. Yao, and X. Xu, *Science* **360**, 1214 (2018).
- [7] W. Xing, L. Qiu, X. Wang, Y. Yao, Y. Ma, R. Cai, S. Jia, X. C. Xie, and W. Han, *Phys. Rev. X* **9**, 011026 (2019).
- [8] X. Wang, J. Tang, X. Xia, C. He, J. Zhang, Y. Liu, C. Wan, C. Fang, C. Guo, W. Yang, Y. Guang, X. Zhang, H. Xu, J. Wei, M. Liao, X. Lu, J. Feng, X. Li, Y. Peng, H. Wei, R. Yang, D. Shi, X. Zhang, Z. Han, Z. Zhang, G. Zhang, G. Yu, and X. Han, *Sci. Adv.* **5**, eaaw8904 (2019).
- [9] S. Ikeda, K. Miura, H. Yamamoto, K. Mizunuma, H. D. Gan, M. Endo, S. Kanai, J. Hayakawa, F. Matsukura, and H. Ohno, *Nat. Mater.* **9**, 721 (2010).
- [10] B. Dieny and M. Chshiev, *Rev. Mod. Phys.* **89**, 025008 (2017).
- [11] F. Katmis, V. Lauter, F. S. Nogueira, B. A. Assaf, M. E. Jamer, P. Wei, B. Satpati, J. W. Freeland, I. Eremin, D. Heiman, P. Jarillo-Herrero, and J. S. Moodera, *Nature (London)* **533**, 513 (2016).
- [12] C. Huang, J. Feng, F. Wu, D. Ahmed, B. Huang, H. Xiang, and E. Kan, *J. Am. Chem. Soc.* **140**, 11519 (2018).
- [13] H. Yang, A. D. Vu, A. Hallal, N. Rougemaille, J. Coraux, G. Chen, A. K. Schmid, and M. Chshiev, *Nano. Lett.* **16**, 145 (2016).
- [14] J. X. Yu and J. Zang, *Sci. Adv.* **4**, eaar7814 (2018).
- [15] J. Liang, W. Wang, H. Du, A. Hallal, K. Garcia, M. Chshiev, A. Fert, and H. Yang, *Phys. Rev. B* **101**, 184401 (2020).
- [16] C. Xu, J. Feng, S. Prokhorenko, Y. Nahas, H. Xiang, and L. Bellaiche, *Phys. Rev. B* **101**, 060404(R) (2020).
- [17] J. Yuan, Y. Yang, Y. Cai, Y. Wu, Y. Chen, X. Yan, and L. Shen, *Phys. Rev. B* **101**, 094420 (2020).
- [18] I. Dzyaloshinskii, *J. Phys. Chem. Solids* **4**, 241 (1958).
- [19] T. Moriya, *Phys. Rev.* **120**, 91 (1960).
- [20] A. Fert, N. Reyren, and V. Cros, *Nat. Rev. Mater.* **2**, 17031 (2017).
- [21] W. Legrand, D. Maccariello, F. Ajejas, S. Collin, A. Vecchiola, K. Bouzehouane, N. Reyren, V. Cros, and A. Fert, *Nat. Mater.* **19**, 34 (2019).
- [22] R. Wiesendanger, *Nat. Rev. Mater.* **1**, 16044 (2016).
- [23] N. Nagaosa and Y. Tokura, *Nat. Nanotechnol.* **8**, 899 (2013).
- [24] J. Sampaio, V. Cros, S. Rohart, A. Thiaville, and A. Fert, *Nat. Nanotechnol.* **8**, 839 (2013).
- [25] S. Yang, R. Peng, T. Jiang, Y. Liu, L. Feng, J. Wang, L. Chen, X. Li, and C. Nan, *Adv. Mater.* **26**, 7091 (2014).
- [26] H. S. Kum, H. Lee, S. Kim, S. Lindemann, W. Kong, K. Qiao, P. Chen, J. Irwin, J. H. Lee, S. Xie, S. Subramanian, J. Shim, S. Bae, C. Choi, L. Ranno, S. Seo, S. Lee, J. Bauer, H. Li, K. Lee, J. A. Robinson, C. A. Ross, D. G. Schlom, M. S. Rzchowski, C. Eom, and J. Kim, *Nature (London)* **578**, 75 (2020).
- [27] L. Caretta, E. Rosenberg, F. Büttner, T. Fakhru, P. Gargiani, M. Valvidares, Z. Chen, P. Reddy, D. A. Muller, C. A. Ross, and G. S. D. Beach, *Nat. Commun.* **11**, 1090 (2020).
- [28] R. O. Cherifi, V. Ivanovskaya, L. C. Phillips, A. Zobelli, I. C. Infante, E. Jacquet, V. Garcia, S. Fusil, P. R. Briddon, N. Guiblin, A. Mougin, A. A. Ünal, F. Kronast, S. Valencia, B. Dkhil, A. Barthélémy, and M. Bibes, *Nat. Mater.* **13**, 345 (2013).
- [29] H. L. Zhuang, P. R. C. Kent, and R. G. Hennig, *Phys. Rev. B* **93**, 134407 (2016).
- [30] J. Son, K.-H. Kim, Y. H. Ahn, H.-W. Lee, and J. Lee, *Phys. Rev. Lett.* **123**, 036806 (2019).
- [31] D. C. Freitas, R. Weht, A. Sulpice, G. Remenyi, P. Strobel, F. Gay, J. Marcus, and M. N.-Regueiro, *J. Phys.: Condens. Matter* **27**, 176002 (2015).
- [32] X. Sun, W. Li, X. Wang, Q. Sui, T. Zhang, Z. Wang, L. Liu, D. Li, S. Feng, S. Zhong, H. Wang, V. Bouchiat, M. N. Regueiro, N. Rougemaille, J. Coraux, A. Purbawati, A. Hadj-Azzem, Z. Wang, B. Dong, X. Wu, T. Yang, G. Yu, B. Wang, Z. Han, X. Han, and Z. Zhang, *Nano Res.* (2020), doi:10.1007/s12274-020-3021-4.
- [33] G. Kresse and J. Hafner, *Phys. Rev. B* **47**, 558 (1993).
- [34] G. Kresse and J. Furthmüller, *Phys. Rev. B* **54**, 11169 (1996).
- [35] G. Kresse and J. Furthmüller, *Comput. Mater. Sci.* **6**, 15 (1996).
- [36] Y. Wang and J. P. Perdew, *Phys. Rev. B* **44**, 13298 (1991).
- [37] G. Kresse and D. Joubert, *Phys. Rev. B* **59**, 1758 (1999).
- [38] B. Yang, X. Zhang, H. Yang, X. Han, and Y. Yan, *Appl. Phys. Lett.* **114**, 192405 (2019).
- [39] X. Sui, T. Hu, J. Wang, B.-L. Gu, W. Duan, and M.-S. Miao, *Phys. Rev. B* **96**, 041410(R) (2017).
- [40] A. Togo and I. Tanaka, *Scr. Mater.* **108**, 1 (2015).
- [41] See Supplemental Material at <http://link.aps.org/supplemental/10.1103/PhysRevB.102.094425> for (1) calculations of  $J, K$ , and DMI; (2) computational details of MC simulations; (3) orbital-resolved band structures of CrXTe monolayers; (4) the difference of spin-orbital angular momentum matrix elements; and (5) the impact of temperature on spin textures of CrSeTe, which includes Refs. [42,51].
- [42] N. Metropolis and S. Ulam, *J. Am. Stat. Assoc.* **44**, 335 (1949).
- [43] O. Boulle, J. Vogel, H. Yang, S. Pizzini, D. de Souza Chaves, A. Locatelli, T. O. Montes, A. Sala, L. D. Buda-Prejbeanu, O. Klein *et al.*, *Nat. Nanotechnol.* **11**, 449 (2016).
- [44] B. Dupe, M. Hoffmann, C. Paillard, and S. Heinze, *Nat. Commun.* **5**, 4030 (2014).
- [45] B. Goodenough, *Phys. Rev.* **100**, 564 (1955).
- [46] J. Kanamori, *J. Phys. Chem. Solids* **10**, 87 (1959).
- [47] P. W. Anderson, *Phys. Rev.* **115**, 2 (1959).
- [48] H. Y. Lv, W. J. Lu, D. F. Shao, Y. Liu, and Y. P. Sun, *Phys. Rev. B* **92**, 214419 (2015).
- [49] D.-S. Wang, R. Wu, and A. J. Freeman, *Phys. Rev. B* **47**, 14932 (1993).
- [50] B. S. Yang, J. Zhang, L. N. Jiang, W. Z. Chen, P. Tang, X.-G. Zhang, Y. Yan, and X. F. Han, *Phys. Rev. B* **95**, 174424 (2017).
- [51] H. Yang, A. Thiaville, S. Rohart, A. Fert, and M. Chshiev, *Phys. Rev. Lett.* **115**, 267210 (2015).
- [52] A. Fert and P. M. Levy, *Phys. Rev. Lett.* **44**, 1538 (1980).
- [53] A. Fert, V. Cros, and J. Sampaio, *Nat. Nanotechnol.* **8**, 152 (2013).